Ballistic electron transport and two-level resistance fluctuations in noble-metal nanobridges

P. A. M. Holweg, J. Caro, A. H. Verbruggen, and S. Radelaar
Delft Institute of Microelectronics and Submicron Technology, Delft University of Technology, Lorentzweg 1, 2628 CJ Delft, The Netherlands
(Received 12 July 1991; revised manuscript received 21 November 1991)

The electrical properties of microfabricated nanobridges of copper, silver, and gold with contact diameters in the range 4–32 nm have been studied. High-quality point-contact spectra are evidence that electron transport is ballistic in these nanobridges. A comparison of our spectra with spectra from mechanical point contacts shows that microfabricated nanobridges are at least as good as mechanical point contacts for study of the electron-phonon interaction. Further, in Au nanobridges we have observed defect motion induced two-level resistance fluctuations (TLF's). An expression is derived for the voltage dependence of the temperature T_d of a defect in a nanobridge at low lattice temperatures. Using this expression for T_d, the experimental voltage dependence of the TLF's is successfully described by a thermal-activation model for the fluctuation rates, in which the voltage dependence of the activation energy and defect temperature is included. The values for the attempt time, activation energy, and electromigration parameter are as expected for defects in metals. An analysis of the two TLF's studied, showing a striking difference in both voltage dependence and magnitude of the duty cycle, suggests that rearrangement of complex defects is the mechanism behind the TLF behavior.

I. INTRODUCTION

Recently microfabrication techniques have been applied to realize metallic point contacts or nanobridges which operate in the ballistic transport regime, where the electron mean free path exceeds the constriction diameter.[1–5] These devices are the microfabricated equivalent of mechanical point contacts and a typical nanobridge has a size between 5 and 30 nm. Ballistic operation of the nanobridges is evident from the high quality of the point-contact spectra. The advantage of microfabricated nanobridges over mechanical point contacts is the excellent mechanical and electrical stability.

This stability and the fact that, in a resistance measurement, one probes a volume of the size of the constriction, make a nanobridge a very suitable system to study the electrical properties of metals on a mesoscopic scale.[2] Ralls and co-workers[1,3] have used nanobridges in this sense and they observed two-level fluctuations (TLF's) in the resistance of Cu, Al, and Pd devices. From their experiments Ralls and co-workers concluded that a TLF in the resistance originates from reversible motion of an atomic scale defect in the constriction region between two metastable states. Depending on the operating conditions of the devices also more defects can be active (more than one TLF in the resistance trace) and, due to the extremely high current density and electric field in the nanobridge, even electromigration of defects can occur (resulting in a changed fluctuation behavior). Ralls and co-workers describe how these fluctuation phenomena can be understood as arising from a "defect glass" system.

In this paper we present experimental data on nanobridges of the noble metals. From a detailed comparison of our point-contact spectra with spectra from the literature recorded with mechanical point contacts, we evaluate our nanobridges as spectroscopic tools. In addition, for the smallest Au bridge we studied TLF's in the resistance at 4.2 K. In contrast to Ralls, Ralph, and Buhrman,[3] who report duty cycles of the TLF's of about 50%, only increasing to 70% for higher voltages, we have observed duty cycles of TLF's in a Au nanobridge that differ considerably. In the analysis of the fluctuation data, the characteristics of the TLF's are related to properties of the defects. Also the magnitude of the resistance change ΔR of the TLF's is discussed in the framework of a theoretical model.

II. FABRICATION AND EXPERIMENTAL TECHNIQUE

The nanobridges are made by evaporating metal onto both sides of a thin (typically 30 nm) silicon nitride membrane with a nanohole. A schematic cross section is shown in Fig. 1. Our fabrication method is very similar to the method presented by Ralls, Buhrman, and Tiberio.[4] The nanohole in the membrane is patterned by electron beam lithography and reactive ion etching. Rotation of the sample during evaporation promotes formation of a clean metal device region in the nanohole. A detailed description of the fabrication process can be found elsewhere.[5]

Point-contact spectra are recorded with a current modulation technique, the dc bias being supplied by a Keithley 220 current source. The voltage across the nanobridge is directly measured with two PAR 5210 lock-in amplifiers. The two signals, corresponding to the first and second derivative of the I-V characteristic, are used to calculate the point-contact spectrum $d^2I/dV^2 = -d^2V/dI^2/(dV/dI)^3$, which is proportional to $\alpha^2F_p(V)$, the point-contact version of the Eliashberg electron-phonon coupling function.[6] For the fluctuation

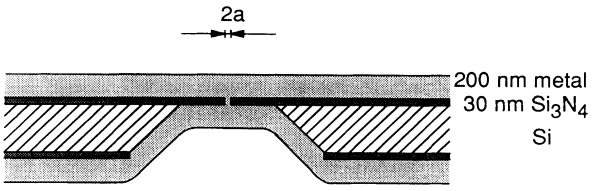

FIG. 1. Cross section of a microfabricated nanobridge. The contact diameter $2a$ is typically 20 nm. A voltage applied across the nanobridge drops almost completely within a distance $2a$ from the center of the device, enabling measurements on an extremely small volume of metal (typically 1000 nm^3).

measurements the nanobridge is only dc biased and time traces of the resistance are recorded after amplifying the voltage fluctuations across the device by a PAR 113 amplifier. The experiment and data acquisition are computer controlled. For measuring the spectral density of the signal a Krohn-Hite 3340 low-pass filter is used. The experimental bandwidth ranged from 1 Hz to 10 kHz.

III. POINT-CONTACT SPECTROSCOPY

Point-contact spectra were recorded of several Cu, Ag, and Au nanobridges. These devices proved to be very stable in time, evidenced by the fact that the resistance of the nanobridge and the quality of the point-contact spectra did not change over periods of weeks. Figure 2 shows a typical spectrum for each metal (solid curves). The spectra show the features characteristic of ballistic devices: a function with well-separated peaks due to transverse-acoustic (TA) and longitudinal-acoustic (LA) phonons, superimposed on a smoothly increasing background that saturates above a certain voltage, i.e., a maximum energy $eV_{\max}$ for phonon creation processes. For comparison, in Fig. 2 we also show spectra of Jansen, Mueller, and Wyder[7] taken from mechanical point contacts (dashed curves), all recorded at $T=1.2$ K. As may be seen, the shape of the spectra from nanobridges in general agrees with that of the mechanical point contacts. In particular the positions of the TA and LA peaks coincide well. The more detailed shape of the Ag nanobridge spectrum in comparison with the mechanical point-contact spectrum is not simply due to the lower measurement temperature. Already at $T=4.2$ K the Ag nanobridge spectrum shows a sharper TA peak than the mechanical point-contact spectrum in Fig. 2. We note that in the spectrum of the Ag nanobridge at the high-energy side of the TA peak a weak shoulder is resolved that corresponds to a similar structure in the phonon density of states measured by Kamitakahara and Brockhouse.[8] This feature is absent in the Ag spectrum of the mechanical point contact.

For each nanobridge the constriction radius was calculated from the resistance at zero bias voltage, given by the Wexler formula[9]

$$R=R_M+R_K=\frac{\rho}{2a}+\frac{4}{3\pi}\frac{\rho l}{a^2}\ , \tag{1}$$

where ρ is the resistivity, a the radius of the constriction, and l the electron mean free path. Equation (1) expresses the resistance as the sum of the Maxwell resistance R_M, that dominates in the diffusive transport regime, and the Knudsen resistance R_K, that dominates in the ballistic transport regime. The elastic mean free path l_e was derived from the residual resistance ratio of a metal strip evaporated simultaneously with the nanobridge. For each device the mean free path amply exceeds the constriction radius, a condition for ballistic operation. The difference between diffusive and ballistic resistance is well illustrated by a comparison between the temperature dependence of the resistance of a nanobridge and bulk metal. A metal strip evaporated simultaneously with the $11-\Omega$ Ag nanobridge (for which the point-contact spectrum is shown in Fig. 2) has a residual resistance ratio $\mathcal{R}=R_{300\ \mathrm{K}}/R_{4.2\ \mathrm{K}}=5.6$. In marked contrast, the $11-\Omega$ Ag nanobridge only drops slightly in resistance when cooled down ($\mathcal{R}=1.1$). This results from the fact that the resistance of the nanobridge is dominated by the ballistic resistance R_K, which is temperature independent

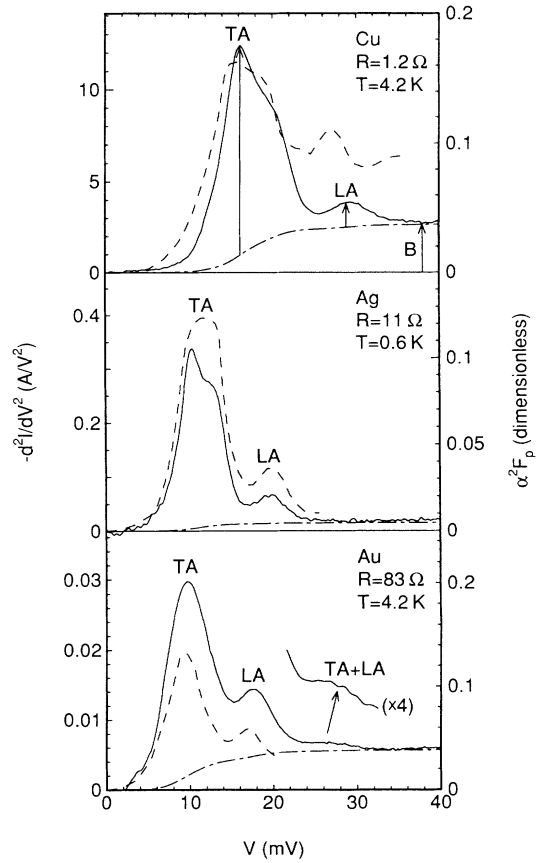

FIG. 2. Point-contact spectra of Cu, Ag, and Au (solid curves) showing transverse-acoustic (TA) and longitudinal-acoustic (LA) phonon peaks. The spectrum of the Au nanobridge shows an additional phonon peak (TA+LA), due to a double-phonon-scattering process. The calculated background signals (dash-dotted curves) are used to determine the peak heights (exemplified by the arrows in the Cu spectrum) listed in Table I. Spectra from mechanical point contacts (Ref. 7) (dashed curves) are shown for comparison. For these point-contact spectra only the α^2F_p scale applies.

(since ρl is temperature independent) and merely a function of geometry (contact radius a).

In the Au spectrum an additional "peak" due to double phonon scattering is resolved at voltage $V_{TA}+V_{LA}$, V_{TA} and V_{LA} being the positions of the TA and LA peaks, respectively. The presence of this peak in the spectrum is evidence of a very clean constriction region. The relative intensity $\mathcal{I}(\mathrm{TA}+\mathrm{LA})/\mathcal{I}(\mathrm{TA})$ of the double phonon peak relative to the TA peak (after subtraction of the background, see below) amounts to 0.04. This is in reasonable agreement with $a/l_e=0.01$, the theoretical value of the relative intensity.[7] We note that for this Au nanobridge the electrical contact between the evaporated Au layers was established by electrically shocking an initially noncontacting nanobridge (all other data presented in Fig. 2 and Table I are from as fabricated nanobridges).

Characteristics of a number of point-contact spectra, including those of Fig. 2, are given in Table I. Entries in the table are nanobridge parameters $\alpha^2F_p(V_{TA})$ (background subtracted), the ratio $\mathcal{I}(\mathrm{LA})/\mathcal{I}(\mathrm{TA})$ of the LA and TA peak intensities (background subtracted), and $\mathcal{I}(\mathrm{B})/\mathcal{I}(\mathrm{TA})$, the ratio of the background (at $V=V_{max}$, as indicated in the Cu spectrum) to the intensity of the TA peak (background subtracted). Numbers in parentheses relate to data taken from the literature. Values of $\alpha^2F_p(V)$ are calculated from[6]

$$\alpha^2F_p(V)=\frac{\hbar}{\pi e^3}\frac{1}{\Omega_{\mathrm{eff}}N(E_F)}\frac{d^2I}{dV^2}(V)\ , \tag{2}$$

where $\Omega_{\mathrm{eff}}=8a^3/3$ is an effective volume wherein phonons are generated[6] and $N(E_F)$ is the electron density of states at the Fermi level. The right-hand scale of Fig. 2 gives units for $\alpha^2F_p(V)$. The background $B(V)$ of the spectra (dash-dotted curves) is obtained by using the function[10] $B(V)=C\int_0^V\alpha^2F_p(V)dV$, where the constant C is taken such that the background level coincides with the spectrum for $V=V_{max}$. To show the dependence of the intensity of the point-contact spectrum on nanobridge resistance, the magnitude of the transverse-acoustic phonon peak for several Ag nanobridges is shown in Fig. 3. From Eqs. (1) and (2) it follows that the intensity d^2I/dV^2 should be proportional to $R^{-3/2}$. From a fit to the data (solid curve in Fig. 3) we find $d^2I/dV^2\propto R^{-1.51}$ in very good agreement with theory.

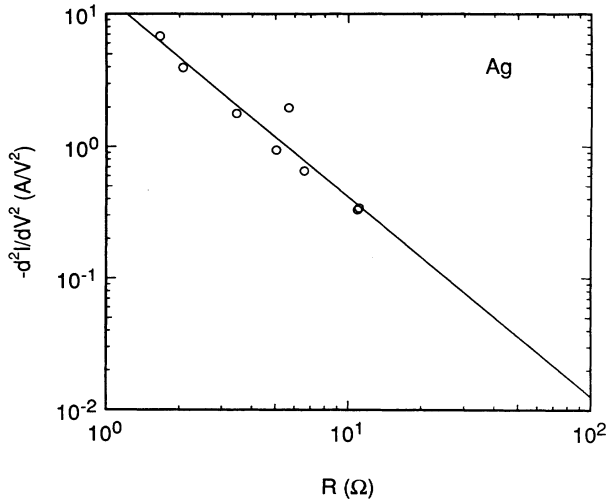

FIG. 3. Magnitude of the transverse-acoustic phonon peak as function of resistance for several Ag nanobridges. The peak height was determined after subtraction of the background at $V=10.5$ mV. The solid curve is a least-squares fit to the data, giving $d^2I/dV^2\propto R^{-1.51}$.

From Table I we observe that $\alpha^2F_p(V_{TA})$ values of the nanobridge spectra agree well with the literature values. The LA peak of the nanobridges is relatively strong and the background relatively low compared with the TA peak, as expected for a ballistic device. In making this comparison we note that for both device types (mechanical point contact and microfabricated nanobridge) varia-

TABLE I. Parameters of six noble-metal nanobridges and of the corresponding spectra. Tabulated are the resistance R, the electron mean free path l_e, the calculated constriction radius a, the intensity $\alpha^2F_p(V_{TA})$ of the transverse-acoustic phonon peak, the ratio $\mathcal{I}(\mathrm{LA})/\mathcal{I}(\mathrm{TA})$ of the intensities of the longitudinal-acoustic and transverse-acoustic phonon peaks, and the ratio $\mathcal{I}(\mathrm{B})/\mathcal{I}(\mathrm{TA})$ of the background signal to the TA phonon peak intensity. Peak heights are determined by subtracting the background signal. Numbers in parentheses relate to literature spectra from mechanical point contacts (Ref. 7).

Material	R (Ω)	l_e (nm)	a (nm)	$\alpha^2F_p(V_{TA})$	Ratio $\mathcal{I}(\mathrm{LA})/\mathcal{I}(\mathrm{TA})$	Ratio $\mathcal{I}(\mathrm{B})/\mathcal{I}(\mathrm{TA})$
copper	1.2[a]	285	16	0.16	0.11	0.23
	2.7	230	11	0.15	0.14	0.12
				(0.12)	(0.29)	(0.68)
silver	11[a]	240	6	0.10	0.17	0.04
	3.4	240	10	0.10	0.13	0.12
				(0.12)	(0.25)	(0.09)
gold	83[a]	140	2	0.19	0.34	0.21
	5.6	140	8	0.14	0.07	0.15
				(0.12)	(0.31)	(0.21)

[a]These parameters correspond to the point-contact spectra of the nanobridges of Fig. 2.

tions in the characteristics of spectra occur from device to device. This is due to differences in crystal orientation and imperfections of the constriction region. Although in this way there is no real standard, we conclude, as judged from the measured spectra, that microfabricated nanobridges as tools to probe the electron-phonon interaction are at least as good as mechanical point contacts of the noble metals. The advantages of nanobridges compared to mechanical point contacts are the high mechanical stability and the absence of degradation of the contact area by oxidation or contamination.

IV. TWO-LEVEL RESISTANCE FLUCTUATIONS

In several gold nanobridges with a relatively high resistance we have observed fluctuations in the resistance as a function of time. For the smallest nanobridge (83 $-\Omega$ Au in Table I) we have studied the fluctuations in detail at 4.2 K. For low biases the fluctuations appear as TLF's ($V=53$ and 59 mV in Fig. 4), the switching rate rapidly increasing with increasing bias. Like Ralls, Ralph, and Buhrman,[3] we find that in this bias range the magnitude and the bias dependence of the fluctuations are reproducible for a specific device (i.e., the device is electrically stable), but differ from device to device, illustrating the mesoscopic character of the nanobridges. At high voltage many fluctuators are active simultaneously ($V=-98$ mV in Fig. 4) and for sufficiently high voltage changes in the average resistance occur. After such an event time traces of the resistance at lower voltages show completely different TLF's. These fluctuation properties are similar to those found by Ralls, Ralph, and Buhrman.[3] In part of the subsequent analysis we will use and elaborate the model of these authors. This model explains the TLF's as originating from reversible motion of a single defect in the constriction region between two metastable states, while the occurrence of a completely different TLF pattern after a resistance change is ascribed to irreversible electromigration of defects.

To study the voltage dependence of the TLF's in more detail we have recorded the spectral density or power spectrum of the fluctuations. Typical spectra for a single TLF at 4.2 K and for three biases are shown in Fig. 5. According to Machlup[11] the power spectrum of a signal that switches randomly between two discrete levels is a Lorentzian given by

$$S_R(f)=\frac{S_0\tau_{\rm eff}}{1+4\pi^2 f^2\tau_{\rm eff}^2}\ , \tag{3}$$

where $S_0/4$ is the integrated power and $\tau_{\rm eff}$ the effective time. These quantities are related to the resistance change ΔR between the levels and to the mean times τ_1 and τ_2 spent in the high and low resistance state, respectively:

$$S_0=4(\Delta R)^2\frac{\tau_{\rm eff}}{\tau_1+\tau_2} \quad \text{and} \quad \frac{1}{\tau_{\rm eff}}=\frac{1}{\tau_1}+\frac{1}{\tau_2}\ . \tag{4}$$

Clearly the shape of the experimental spectra is close to the Lorentz function, that is constant for low frequencies and starting from a knee frequency rolls off as $1/f^2$. For further analysis we fitted to the data a Lorentzian plus a $1/f$ term to describe the small residual noise originating from the preamplifier and possibly from the nanobridge. This linear combination describes the data excellently. The resulting Lorentzians are shown in Fig. 5. Even at

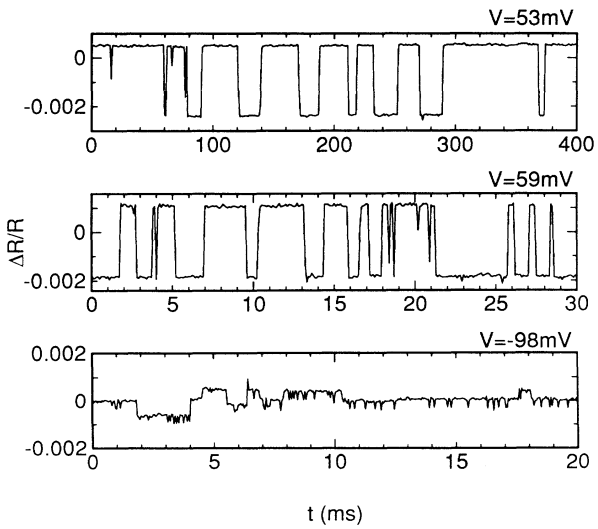

FIG. 4. Time traces of resistance fluctuations of the 83-Ω Au nanobridge of Fig. 2, at 4.2 K and for three biases. The switching rate of the two-level fluctuator increases if the bias is raised from 53 to 59 mV. At relatively high voltages more fluctuators are visible simultaneously, as can be seen in the -98-mV time trace.

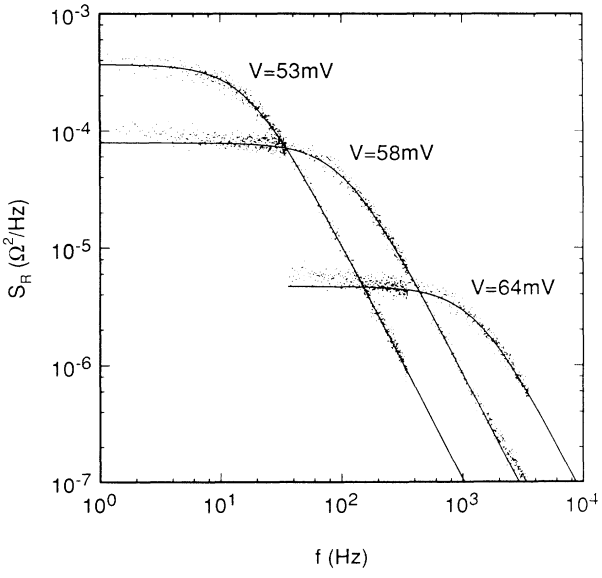

FIG. 5. Spectral density of a single two-level fluctuator for three bias voltages, illustrating the Lorentzian line shape. The spectra were taken at 4.2 K from the Au nanobridge for which time traces are shown in Fig. 3. Due to defect heating the knee of the Lorentzian shifts to higher frequency for larger bias. The curves are the resulting Lorentzian spectra obtained by fitting a Lorentzian plus a $1/f$ term to account for the small residual $1/f$ noise.

300 K TLF's can be distinguished in the time traces (see Fig. 6), but many of them are active simultaneously and over longer periods of time new TLF's enter the experimental bandwidth while others disappear. The inset of Fig. 6 shows a typical power spectrum of fluctuations of a nanobridge at 300 K. This is a typical $1/f$ noise spectrum usually characterized by the phenomenological Hooge equation[12] $S_R(f)/R^2=\gamma/(Nf^\alpha)$, wherein γ and α are fit parameters, and N is the number of charge carriers, taken equal to the effective volume $4\pi a^3/3$ of the nanobridge times the electron density. To allow a comparison of the noise magnitude of the nanobridges with the noise magnitude of metal films, the noise from nanobridges is scaled with the diffusive part R_M of the total nanobridge resistance.[13] In this way, the fluctuations are not attributed to changes in the geometry of the nanobridge (corresponding to changes in the ballistic resistance) as function of time. The equivalent scaling formula for the noise magnitude in a nanobridge then becomes

$$\gamma=\frac{S_R(f)Nf^\alpha}{R_M^2} . \tag{5}$$

For the nanobridge, of which the power spectrum is shown in the inset of Fig. 6, we calculate $R_M=4.3\ \Omega$ at room temperature using Eq. (1) and the resistivity of Au. A fit of Eq. (5) to the 300-K spectrum gives $\gamma=5.6\times10^{-3}$ and $\alpha=1.2$. The slope α is in the range 0.9–1.4 generally observed in $1/f$ noise.[14] The intensity γ, which depends both on the $(1/f)$-noise generating mechanism and specific device characteristics, falls in the range usually found for $1/f$ noise in metal films.[15] We conclude that our measurements provide additional evidence for the theory that $1/f$ noise in metals originates from a superposition of Lorentzians, each of them characterizing the noise due to motion of a single defect.

In the analysis of the voltage dependence of two TLF's at 4.2 K we derived the mean times τ_1 and τ_2 from Eq. (4) using the parameters of the fitted Lorentzians and the magnitude of the resistance changes. The results are plotted in Fig. 7 as function of 1/voltage. The fluctuation rates for both TLF's increase rapidly with increasing voltage. The high and low resistance states of TLF1 respond differently to the voltage. In our experimental bandwidth the duty cycle $\tau_1/(\tau_1+\tau_2)$ decreases rapidly from 80% to 20% between 53 and 64 mV. For negative sample biases TLF1 was not observed. TLF2 is active at lower voltages, both positive and negative. Its duty cycle is fairly constant but small (7%). These duty cycle properties are completely different from those reported by Ralls, Ralph, and Buhrman,[3] who only observed duty cycles of about 50%, changing only to 70% for higher voltage.

Random switching between discrete resistance levels in a nanobridge is caused by a defect jumping back and forth in a double-well potential.[3] The increase in fluctuation rate with increasing bias voltage suggests a thermally activated behavior, involving a defect temperature T_d depending on bias voltage. We will discuss if overall sample heating can explain the voltage dependence of T_d. The TLF's are observed in a nanobridge with a high-quality point-contact spectrum (see Fig. 2), which shows a double phonon peak in the voltage range where the TLF's are observed. Thermal broadening caused by sample heating would make this observation impossible. However, it was shown that sample heating is significant in diffusive point contacts, but is always accompanied by a large background in the point-contact spectrum.[16] Our small back-

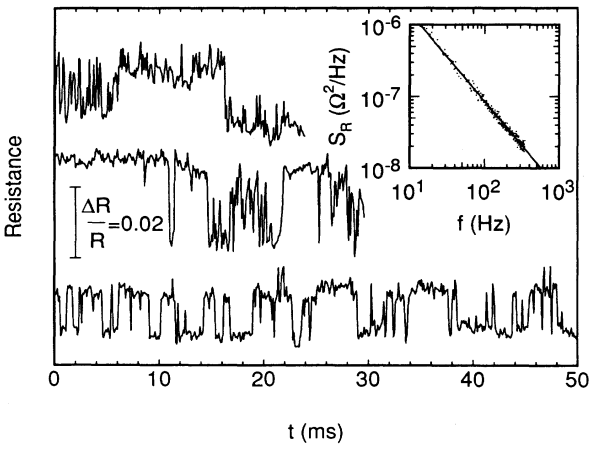

FIG. 6. Resistance vs time for a 1.2-kΩ Au nanobridge at 300 K and at 12-mV bias. The time traces (which are offset for clarity) were taken under identical conditions. The interval between time traces was a few seconds. At 300 K switching between discrete resistance levels is still visible but the character of the noise changes in time. The inset shows a typical spectral density of the fluctuations of a 54-Ω nanobridge at 300 K and at 16-mV bias, illustrating the $1/f$ character of the noise.

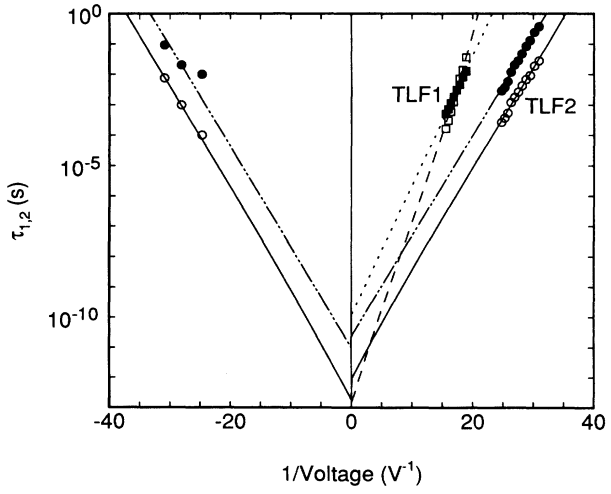

FIG. 7. Mean times spent in one of the resistance states of TLF1 and TLF2 observed in a Au nanobridge at 4.2 K as a function of 1/voltage. Open (closed) symbols denote the high (low) resistance state. The solid lines are fits to the data points and yield the defect parameters listed in Table II. The slope gives the activation energy, the mean y-axis intercept gives the attempt time, while the difference in y-axis intercept between the positive and negative voltage branch is a measure of the electromigration force.

ground signal proves that the nanobridges are not in this diffusive regime. Moreover, in case of overall sample heating the fluctuation behavior should be identical for reversal of voltage polarity. This is in disagreement with the observed asymmetries of the fluctuations rates of the TLF's. The inconsistency of the TLF behavior with overall sample heating is further evidenced by Ralls, Ralph, and Buhrman,[3] who found that the duty cycle of a TLF remains constant as a function of temperature, while it changes as a function of voltage. Therefore we conclude that the voltage dependence of a TLF cannot be explained by overall sample heating.

We explain the TLF behavior by local heating of the defect above the lattice temperature due to inelastic scattering with ballistic electrons. The usual thermally activated behavior of the mean time τ_i $(i=1,2)$ is modified to take into account the electromigration force on the defect:

$$\tau_i=\tau_{0i}\exp\left[\frac{\varepsilon_i-\zeta_i V}{kT_d}\right] . \tag{6}$$

Here τ_{0i} is the attempt time, ε_i the activation energy, ζ_i the electromigration parameter, V the voltage, and T_d the bias-dependent defect temperature. The parameter ζ_i measures the total change of activation energy of the defect as a result of the electromigration force[17] (direct force plus wind force) and causes an asymmetry of the $\log_{10}(\tau_i)$ versus $1/V$ plot. The temperature of a defect in a nanobridge can be higher than the lattice temperature, because electrons can be accelerated to high enough energies to scatter inelastically with a defect, which is unique for the nanobridge geometry. To derive an expression for the defect temperature for high bias voltage and low lattice temperature, we adapted the approach of Ref. 3. The defect is assumed to be coupled only to the electrons, so that in equilibrium the requirement of zero net power transfer P from the electrons to the defect, both by energy gain and energy loss, is

$$P\propto\sum_{\mathbf{k}}\sum_{\mathbf{k}'}(E_{\mathbf{k}}-E_{\mathbf{k}'})f_{\mathbf{k}}(1-f_{\mathbf{k}'})S(\mathbf{Q},E_{\mathbf{k}}-E_{\mathbf{k}'})=0 , \tag{7}$$

where $\mathbf{Q}=\mathbf{k}'-\mathbf{k}$ is the scattering vector of an electron between initial state $\mathbf{k}$ and final state $\mathbf{k}'$, $E_{\mathbf{k}}-E_{\mathbf{k}'}$ is the energy transfer in the scattering process, $f_{\mathbf{k}}$ is the electron distribution function for the ballistic nanobridge geometry, and $S(\mathbf{Q},E_{\mathbf{k}}-E_{\mathbf{k}'})$ the scattering function for electrons colliding with the defect. When the defect is modeled by an isotropic harmonic oscillator with level spacing $\hbar\omega_d$, then $S(\mathbf{Q},E_{\mathbf{k}}-E_{\mathbf{k}'})$ takes the form[18]

$$S(\mathbf{Q},\hbar\omega)=e^{-2W}e^{\hbar\omega/2kT_d}\sum_{n=-\infty}^{\infty}I_n(y)\delta(\hbar\omega-n\hbar\omega_d) , \tag{8}$$

where e^{-2W} is the Debye-Waller factor and $I_n(y)$ is a modified Bessel function of the first kind. Both W and y can be expressed in the zero-point motion amplitude $\langle 0|\hat{\mathbf{r}}^2|0\rangle^{1/2}$ of the harmonic oscillator:

$$W=\tfrac{1}{6}\langle 0|\hat{\mathbf{r}}^2|0\rangle\mathbf{Q}^2\coth\left[\frac{\hbar\omega_d}{2kT_d}\right] , \tag{9}$$

$$y=\tfrac{1}{3}\langle 0|\hat{\mathbf{r}}^2|0\rangle\mathbf{Q}^2\operatorname{csch}\left[\frac{\hbar\omega_d}{2kT_d}\right] . \tag{10}$$

Since the zero-point motion amplitude is much smaller than the interatomic distance the Debye-Waller factor $e^{-2W}\approx 1$, while for the Bessel function the small argument expansion $I_n(y)\approx(y/2)^{|n|}(|n|!)$ can be used. Consequently, we only need to retain the $n=\pm 1$ terms in the expression for $S(\mathbf{Q},\hbar\omega)$, corresponding to creation and annihilation of a quantum of energy $\hbar\omega_d$. As a result the scattering function can be greatly reduced and Eq. (7) takes the form

$$P\propto\sum_{\mathbf{k}}\sum_{\mathbf{k}'}(E_{\mathbf{k}}-E_{\mathbf{k}'})f_{\mathbf{k}}(1-f_{\mathbf{k}'})\mathbf{Q}^2[(n_0+1)\delta(\hbar\omega-\hbar\omega_d)+n_0\delta(\hbar\omega+\hbar\omega_d)]=0, \tag{11}$$

where $n_0=[\exp(\hbar\omega/kT_d)-1]^{-1}$ is the Bose-Einstein distribution function. Finally, for a defect in the center of the nanobridge we derive from Eq. (11) for the low lattice temperature limit the simple relation

$$kT_d=\frac{\hbar\omega_d}{\ln[1+16\hbar\omega_d/5(e|V|-\hbar\omega_d)]} . \tag{12}$$

By numerically solving Eq. (11), it can be shown that the validity of this low-temperature expression is still excellent at 4.2 K, so that it is well suited for our measurement data. For energies $e|V|$ much larger than $\hbar\omega_d$, Eq. (12) reduces even further to

$$kT_d=\tfrac{5}{16}e|V| , \tag{13}$$

so that the defect temperature becomes completely independent of specific defect parameters.

We used Eq. (12) for the defect temperature to fit the thermal activation model represented by Eq. (6) to the mean times shown in Fig. 7. Contrary to Ralls, Ralph, and Buhrman,[3] we did not fix the harmonic oscillator frequency ω_d in our calculation but linked it to the attempt time by $\omega_d=2\pi/\tau_0$. Lacking data at negative biases for TLF1, $\zeta_{1,2}$ was set to zero for this fluctuator. As shown in Fig. 7, the fitted curves describe the data very well. Since T_d is proportional to V [as can be seen from Eq. (13)], $\log_{10}(\tau_{1,2})$ is proportional to $1/V$, expressing the thermally activated behavior of the defect motion. In Fig. 7 the slope is a measure of the activation energy, the mean y-axis intercept gives the attempt time, while the difference in y-axis intercept between the positive and negative voltage branch is proportional to the electromigration force on the defect. Fitted parameters and other characteristics of TLF1 and TLF2 are compiled in Table II. The parameters ε_i, ζ_i, and Z_i^* are upper limits because the actual defect temperature will be smaller than calculated for two reasons. First, we assumed the defect to be centered in the nanobridge. Second, we did not take into account that the defect will lose energy to the

TABLE II. Defect parameters of fluctuators TLF1 and TLF2 observed in a Au nanobridge. The quantity $\Delta R/R$ is the measured relative resistance change and $\Delta\sigma$ is the corresponding change in scattering cross section. The table gives the attempt time τ_0, activation energy ε, electromigration parameter ζ, and effective valence Z^* for the two resistance states of the defect. The values of the last three parameters are upper limits, as discussed in the text. For TLF1 ζ could not be determined and was set to zero in the fit (see text).

Fluctuator	$\frac{\Delta R}{R}$	$\Delta\sigma$ (nm^2)	Resistance state	τ_0 (s)	ε (meV)	ζ (meV/mV)	Z^*
TLF1	2.7×10^{-3}	3.7×10^{-3}	high	$10^{-13.0}$	453		
			low	$10^{-9.9}$	308		
TLF2	3.8×10^{-4}	5.2×10^{-3}	high	$10^{-12.4}$	275	−0.25	−3.5
			low	$10^{-10.8}$	239	−0.13	1.9

lattice. However, as shown by Ralls, Ralph, and Buhrman,[3] the effect of energy relaxation to the lattice for low lattice temperatures is simply a scaling factor for the defect temperature. Therefore fitted values of the activation energy ε_i and the electromigration parameter ζ_i will scale with the same factor. If we adopt the value of the relaxation parameter experimentally found by Ralls, Ralph, and Buhrman,[3] our values for ε_i and ζ_i listed in Table II will be reduced by a factor of approximately 2. The values of τ_{0i} in Table II correspond to typical phonon frequencies and ε_i values are as expected for defect motion in metals.[19] Our values of the parameters τ_{0i}, ε_i, and ζ_i are in the same range as found in Ref. 3, confirming the results of that work. There is, however, also a remarkable difference with Ref. 3. For TLF1 namely, both τ_{0i} and ε_i differ considerably for the high and low resistance state, meaning than the double-well potential is highly asymmetric. This indicates that we deal here with a relatively complex defect that does not simply jump between two equivalent positions or orientations (such as a vacancy changing site). At the point $\tau_1=\tau_2$ in Fig. 7 the bias-induced defect heating is strong enough to make the exponentials in Eq. (6) compensate for the different attempt times. The absence of TLF1 for negative biases may be due to the fact that ζ_1 and ζ_2 differ in such a way that the difference in effective activation energy (i.e., $\varepsilon_i-\zeta_i V$) is even increased for this polarity. In that case the rates $1/\tau_1$ and $1/\tau_2$ may differ so much that the TLF's cannot both be observed in the experimental bandwidth. For TLF2, on the other hand, ε_1 and ε_2 are more equal. So in this case the double well is more symmetric. The small duty cycle is due to the difference in attempt time for the two states. From the fitted ζ_i values a crude estimate can be made for the effective valence Z_i^*. In doing so, we assume that the defect jumps a nearest-neighbor distance d (in Au $d=0.29$ nm) along the central axis of the nanobridge. The effective valence is then given by $Z_i^*=2a\zeta_i/d$. The resulting values in Table II are quite reasonable for the effective valence of atomic-size defects.

The last property of the TLF's we address is the resistance change ΔR between the high and low resistance states. We have found that the magnitude of the resistance change of a particular fluctuator is independent of voltage, but changes from fluctuator to fluctuator. In our experiments on Au nanobridges the relative change $\Delta R/R$ ranged from 2×10^{-4} to 3×10^{-3}. In order to discuss the magnitude of the resistance changes, we derive an expression for $\Delta G=-\Delta R/R^2$ from the formula of Sorbello[20] for the change in current ΔI due to the introduction of an impurity at position $\mathbf{r}_0$ in a ballistic nanobridge:

$$\Delta I=-\frac{e^2V\Omega^2}{16\pi^5\hbar^3v_F^2}\int_{\mathbf{k}\in\Omega_0(\mathbf{r}_0)}dS_{\mathbf{k}}\int_{\mathbf{k}'\in\Omega_o^*(\mathbf{r}_0)}dS_{\mathbf{k}'}|T_{\mathbf{k}\mathbf{k}'}|^2\,. \tag{14}$$

In Eq. (14) V is the voltage, Ω the volume, v_F the Fermi velocity, and $T_{\mathbf{k}\mathbf{k}'}$ is an element of the T matrix for impurity scattering. The integrals over the Fermi surface are restricted to solid angles. These define zones on the Fermi surface with electrons that arrive at $\mathbf{r}_0$ after having traversed the constriction $[\Omega_0(\mathbf{r}_0)]$ or that are backscattered from $\mathbf{r}_0$ into the direction of the constriction $[\Omega_0^*(\mathbf{r}_0)]$. We now assume that the current changes ΔI_1 and ΔI_2 for either position of a defect causing a TLF are given by Eq. (14), so that ΔG is proportional to $\Delta I_1-\Delta I_2$. The conductance can change in two ways. First, a difference in scattering properties of the two metastable states, as expressed by a different $|T_{\mathbf{k}\mathbf{k}'}|$ for each state, will cause a conductance change. Second, the mere positional change of the defect will cause a conductance change, since the solid angles and therefore the number of electrons that arrive at the impurity after traversing the constriction and subsequently scatter back through the constriction will be different for each state. To gain insight into the relative importance of the two contributions, the magnitude of the conductance changes attainable by the two above-mentioned mechanisms will be estimated. As an approximation for $|T_{\mathbf{k}\mathbf{k}'}|$ we take the usual Legendre polynomial expansion of which we only keep the lowest-order term. This means that we assume isotropic scattering. Then with $|T_{\mathbf{k}\mathbf{k}'}|=(2\pi\hbar^2/mk_F\Omega)\sin\delta_0$, m being the electron mass, we find

$$\Delta G=-\frac{\Delta R}{R^2}=-\frac{2e^2}{h}\frac{[\Omega_0(\mathbf{r}_1)\Omega_0^*(\mathbf{r}_1)\sin^2\delta_{01}-\Omega_0(\mathbf{r}_2)\Omega_0^*(\mathbf{r}_2)\sin^2\delta_{02}]}{4\pi^2}\,. \tag{15}$$

With our assumption of isotropic scattering Eq. (15) gives an upper bound $2e^2/h$ for a conductance change of a TLF. Our observed conductance changes are of the same order but always smaller than this value. To judge the accuracy of our isotropic approximation, the conductance change ΔG was calculated for a single scatterer centered in a nanobridge, starting from Eq. (14) and including the first four terms of the Legendre polynomial expansion. By taking for the scatterer a vacancy in a Ag or Al lattice, we find that the approximation of isotropic scattering for these defects is accurate to within a factor of 5. To estimate the magnitude of the conductance change of a TLF attainable by positional change of a defect, we will calculate the ΔG of a defect jumping one lattice spacing and having identical scattering properties in both states (i.e., $\delta_{01}=\delta_{02}$). The strongest dependence of $\Delta G(\mathbf{r}_1,\mathbf{r}_2)$ on the positions is on the axis of the nanobridge, close to the center of the device. Consequently, the largest conductance change is obtained by a jump direction along the axis of the nanobridge, by setting $\delta_{0i}=\pi/2$ and taking one of the defect positions as the center of the nanobridge (we then have $\Omega_0(\mathbf{r}_i)=2\pi[1-z_i/(a^2+z_i^2)^{1/2}]$ with z_i the position on the axis). Taking as a reasonable jump distance the nearest-neighbor distance (0.29 nm in Au) and using $a=2$ nm for our 83-Ω nanobridge Eq. (15) then gives a conductance change $\Delta G=0.5e^2/h$, which is of the same order as the maximum observed conductance change ($\Delta G=0.84e^2/h$ for TLF1). Therefore the change in position of a defect between two metastable states can contribute substantially to the total conductance change of the TLF's. To investigate the influence of a difference in scattering properties of the defect between its two states, we will consider the case where ΔG originates entirely from a reorientation of a defect and we will calculate the accompanying change in scattering cross section $\Delta\sigma$. Then, ignoring any position dependence by centering the defect in the constriction for both defect states and using $\sigma_i=(4\pi/k_F^2)\sin^2\delta_{0i}$, we find from Eqs. (15) and (1)

$$\Delta\sigma=\sigma_1-\sigma_2=-\frac{h}{2e^2}\frac{4\pi}{k_F^2}\Delta G\approx\pi a^2\frac{\Delta R}{R}\ . \tag{16}$$

Values of $\Delta\sigma$ for TLF1 and TLF2 calculated from this equation are listed in Table II. These values represent lower limits on $\Delta\sigma$, because a TLF further away from the constriction center requires a larger $\Delta\sigma$ to cause the same conductance change as a centered TLF. The obtained values for $\Delta\sigma$ are reasonable for defects with atomic dimensions. We conclude that a positional change of a defect between two metastable states as well as a change in scattering cross section between these two states are important in explaining the magnitude of the conductance change of a TLF in a nanobridge.

An important and so far unresolved question in the observed noise behavior of the nanobridges is what type of defects causes the two-level resistance fluctuations. The stability of the discrete resistance levels rules out single point defects, such as single vacancies or interstitials, because there is no apparent reason why these types of defects would jump between only two metastable positions. Rather one would expect these defects to diffuse through the lattice. The magnitude of the resistance changes, the activation energies, and the attempt times of the fluctuations and the stability of the fluctuation levels all suggest that TLF's are caused by complex defects that are sufficient strongly bound to the lattice. The reorientation of such a complex defect could very well explain the difference in attempt times and activation energies of the two states. In the scattering of electrons with complex defects quantum interference will play an important role. The positional change and reorientation of defects as discussed above explain many characteristics of the observed TLF behavior, but for a detailed description a more elaborate model will be required. Recently, resistance fluctuations in small metallic samples have been discussed[21] as originating from electron interference, specifically in the framework of the universal conductance fluctuations (UCF) and local interference (LI) models. Since the UCF model applies to the diffusive transport regime, the LI model[22] should be more appropriate for the ballistic nanobridges.

V. CONCLUSIONS

In conclusion, we have fabricated ballistic noble-metal nanobridges, from which high-quality nanobridge spectra were obtained and which showed two-level resistance fluctuations induced by reversible defect motion. The very small effective volume (typically 1000 nm^3), together with the extremely high current density (10^9 A/cm^2) and electrical field (10^5 V/cm) attainable in nanobridges, allows the study of defect properties from the bias dependence of the fluctuations. The device characteristics make nanobridges a powerful tool in the study of the detailed microscopic mechanisms of $1/f$ noise and electromigration. Specifically, the determination of the effective valence of a defect from the asymmetry of the bias dependence of the fluctuation rate shows that electromigration parameters can be obtained. Further, the observation at room temperature of resistance fluctuations with many TLF's active simultaneously and resulting in a $1/f$ power spectrum demonstrates that the defect motion, visible at 4.2 K as a single TLF with Lorentzian spectrum, is a fundamental mechanism of $1/f$ noise. The nature of the defect parameters and the result of an evaluation of the magnitude of the resistance changes suggest that complex defects are involved in the fluctuation phenomena. Moreover, the local interference model could provide an appropriate description for the TLF behavior. For better insight into electromigration and $(1/f)$-noise processes, it would be interesting to introduce and study well-known defects in a nanobridge.

ACKNOWLEDGMENTS

We would like to thank H. M. Jäger for stimulating discussions. Further we wish to acknowledge C. Visser for depositing the silicon nitride layers and H. Postma for providing experimental facilities. This work is part of the research program of the Stichting Fundamenteel Onderzoek der Materie (FOM), which is financially supported by the Nederlandse Organisatie voor Wetenschappelijk Onderzoek (NWO).

[1]K. S. Ralls and R. A. Buhrman, Phys. Rev. Lett. **60**, 2434 (1988).
[2]P. A. M. Holweg, J. A. Kokkedee, J. Caro, A. H. Verbruggen, S. Radelaar, A. G. M. Jansen, and P. Wyder, Phys. Rev. Lett. **67**, 2549 (1991).
[3]K. S. Ralls, D. C. Ralph, and R. A. Buhrman, Phys. Rev. B **40**, 11 561 (1989).
[4]K. S. Ralls, R. A. Buhrman, and R. C. Tiberio, Appl. Phys. Lett. **55**, 2459 (1989).
[5]P. A. M. Holweg, J. Caro, A. H. Verbruggen, and S. Radelaar, Microelectron. Eng. **11**, 27 (1990).
[6]I. O. Kulik, A. N. Omel'yanchuk, and R. I. Shekhter, Fiz. Nizk. Temp. **3**, 1543 (1977) [Sov. J. Low Temp. Phys. **3**, 740 (1977)].
[7]A. G. M. Jansen, F. M. Mueller, and P. Wyder, Phys. Rev. B **16**, 1325 (1977).
[8]W. A. Kamitakahara and B. M. Brockhouse, Phys. Lett. **29A**, 639 (1969).
[9]G. Wexler, Proc. Phys. Soc. **89**, 927 (1966).
[10]I. K. Yanson and A. G. Batrak, Zh. Eksp. Teor. Fiz. **76**, 325 (1979) [Sov. Phys. JETP **49**, 166 (1979)].
[11]S. Machlup, J. Appl. Phys. **25**, 341 (1954).
[12]F. N. Hooge, Phys. Lett. **34A**, 139 (1969).
[13]K. S. Ralls and R. A. Buhrman, Phys. Rev. B **44**, 5800 (1991).
[14]P. Dutta and P. M. Horn, Rev. Mod. Phys. **53**, 497 (1981).
[15]J. H. Scofield, J. V. Mantese, and W. W. Webb, Phys. Rev. B **32**, 736 (1985).
[16]I. K. Yanson, Fiz. Nizk. Temp. **9**, 676 (1983) [Sov. J. Low Temp. Phys. **9**, 343 (1983)].
[17]A. H. Verbruggen, IBM J. Res. Dev. **32**, 93 (1988).
[18]W. Marshall and S. W. Lovesey, *Theory of Thermal Neutron Scattering* (Oxford University Press, Oxford, 1971), p. 57.
[19]J. Pelz and J. Clarke, Phys. Rev. Lett. **55**, 738 (1985).
[20]R. S. Sorbello, Phys. Rev. B **39**, 4984 (1989).
[21]N. Giordano and E. R. Schuler, Phys. Rev. B **41**, 11 822 (1990); N. Giordano, in *Mesoscopic Phenomena in Solids*, edited by B. L. Al'tschuler, P. A. Lee, and R. Webb (North-Holland, Amsterdam, 1991).
[22]J. Pelz and J. Clarke, Phys. Rev. B **36**, 4479 (1987).

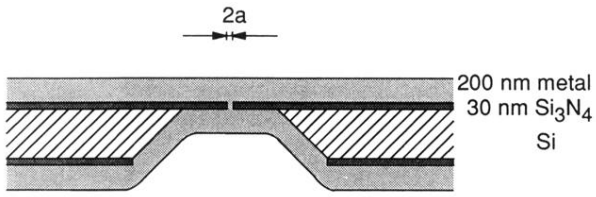

FIG. 1. Cross section of a microfabricated nanobridge. The contact diameter $2a$ is typically 20 nm. A voltage applied across the nanobridge drops almost completely within a distance $2a$ from the center of the device, enabling measurements on an extremely small volume of metal (typically 1000 nm^3).